Shear wave anisotropy beneath the volcanic front in South Kyushu area, Japan: Development of C-type olivine CPO under H2O-rich conditions

Shear wave anisotropy beneath the volcanic front in south Kyushu area, Japan:

Development of C-type olivine CPO under H$_2$O-rich conditions

Tadashi Terada[1], Yoshihiro Hiramatsu[2], and Tomoyuki Mizukami[2]

[1]Graduate School of Natural Science and Technology, Kanazawa University

Kakuma, Kanazawa, 920-1192, Japan

[2]School of Natural System, College of Science and Engineering, Kanazawa University

Kakuma, Kanazawa, 920-1192, Japan

Corresponding author:

Yoshihiro Hiramatsu

Kakuma, Kanazawa, 920-1192, Japan

e-mail: yoshizo@hakusan.s.kanazawa-u.ac.jp

phone: +81-76-264-6519

fax: +81-76-264-6545

Abstract

Shear wave splitting from local intermediate-depth earthquakes is investigated to detect the anisotropic structure in the mantle wedge beneath the south Kyushu area, Japan. We observed shear wave splitting with NEE–SWW to NWW–SEE polarization directions and delay times of 0.04–0.63 s. Trench-normal shear wave polarization anisotropy with delay time greater than 0.3 s probably overlaps in the high V_P/V_S region at the depth of 100–150 km beneath the volcanic front. Model calculations for the cause of the anisotropy suggest that the development of 'C-type' olivine crystallographic preferred orientation (CPO) with a trench-parallel b-axis concentration and a trench-normal a-axis concentration best reproduces observations compared to A-, B- or E-type olivine CPOs and antigorite CPO. We conclude that a thick anisotropic layer, approx. 50 km, is formed by concentration of interstitial fluid in peridotite. We briefly discuss the mechanism carrying water to the deep mantle wedge. A possible explanation is that interstitial fluids in the mantle wedge are effectively released because of a decrease of dihedral angles of olivine-fluid interfaces at 150 km depth. Our results imply a close relation between the high density of explosive volcanoes in the south Kyushu area and the underlying water-rich mantle.

1. Introduction

Fluid mobility and its distribution are important factors of subduction dynamics such as seismicity, magmatism, and metamorphism. For example, fluid reduces the melting point of rocks and causes melt formation, leading to volcanic activity [e.g., *Green*, 1973; *Niida and Green*, 1999; *Grove et al*., 2009]. Fluid in the mantle wedge transforms olivine to hydrous minerals such as serpentine under temperature conditions along subduction boundaries [*Ulmer and Trommsdorff*, 1999; *Hyndman and Peacock*, 2003]. Experimental studies show that shear deformation under water-rich condition causes crystallographic preferred orientation (CPO) of olivine, the most dominant and strongly anisotropic mineral in the upper mantle [e. g., *Karato et al*., 2008]. In addition, single-crystal serpentine (antigorite) generates strong seismic anisotropy up to 72% [*Bezacier et al*., 2010; *Mookherjee and Capitani,* 2011] and, therefore, development of foliated antigorite serpentinite can be a cause of mantle anisotropy [*Katayama et al*., 2009; *Soda and Takagi,* 2010; *Hirauchi et al.,* 2010; *Jung*, 2011; *Nishii et al.*, 2011; *Padrón-Navarta et al.*, 2012]. The recent knowledge of physical properties of mantle minerals suggests that the extents of hydration and fluid distributions in mantle wedge

can be examined based on detailed observations of seismic anisotropy and seismic velocity in the mantle wedge.

A shear wave propagating in anisotropic media splits into two orthogonal polarizations, one wavelet traveling faster than the other. Shear wave splitting, which is expressed by the orientation of the fast polarization, φ, and the delay time or the time difference of two split shear waves, δt, from local intermediate-depth and/or deep earthquakes, has been a powerful tool to observe anisotropic structures in subduction zones [e.g. *Ando et al.*, 1980]. Combination of shear wave splitting data from local and teleseismic earthquakes provides information about the vertical distribution of seismic anisotropy beneath convergent margins, that is, in a mantle wedge [*Long and van der Hilst*, 2005], within a slab [*Faccenda et al.*, 2008], and below a slab [*Russo and Silver*, 1994; *Long and Silver*, 2009].

Dense observations of shear wave splitting from local intermediate-depth and/or deep earthquakes have provided a heterogeneous spatial distribution in splitting parameters in the mantle wedge [e.g. *Hiramatsu et al.*, 1998; *Nakajima and Hasegawa*, 2004]. In several subduction zones (e.g., northeastern (NE) Japan, the Ryukyu, and New Zealand), the orientation of the fast wave propagated in the mantle wedge is characteristically parallel to the strike of the trench, especially in the forearc region [e.g.

Nakajima and Hasegawa, 2004; *Long and van der Hilst*, 2005; *Greve et al.*, 2008]. This seismic anisotropy is termed as trench-parallel anisotropy. However, an example of a trench-normal anisotropy, φ is normal to the strike of the trench, beneath a volcanic front and a trench-parallel anisotropy beneath the back-arc mantle is reported from Kamchatka peninsula [*Levin et al.*, 2004]. This implies that nature of mantle wedge anisotropy is more complicated than recent interpretations that simply separate the polarization orientation into the trench-parallel and trench-normal components.

We focus on the south Kyushu area located at the northern end of the Ryukyu arc (Figure 1). This area is characterized by a high concentration of active volcanoes. The Quaternary records of huge pyroclastic flows [e.g., *Aramaki*, 1984] and depositions of tephra almost covering the Japanese islands [*Machida*, 1999] represent anomalously explosive eruptions of volatile-rich magmas probably supplemented by a fluid source underneath. Tomographic studies clearly show a high V_P/V_S region at the depths of 100-150 km in the mantle wedge (Figure 1) [*Matsubara et al.*, 2008; *Matsubara and Obara*, 2011]. This region is also characterized by low V_P and low V_S. Detailed observations of shear wave splitting and its spatial distribution will show us new substantial aspects of the seismologically and geologically anomalous region and will help our understanding of the mantle wedge.

Long and van der Hilst [2006] reported the trench-parallel orientation of φ in the mantle wedge in the Ryukyu arc from analyses of long-period seismic wave data from local intermediate-depth earthquakes. However, their discussion is based mainly on the results of the average orientation of φ at each station even where their data show a large variability. More recently *Salah et al.* [2009] analyzed shear wave splitting in this region and obtained that fast polarization axes dominantly trend E-W. They found that there is no significant difference between the φ data in the fore-arc region and those in the back-arc. The discrepancy between the previous studies is possibly due to a complex structure of the mantle. Therefore, as suggested by *Salah et al.* [2009], more detailed 3D analyses and reliable dataset based on careful examination of seismic waveforms are still necessary.

In this study, we analyze shear wave splitting of local intermediate-depth earthquakes of the subducting Philippine Sea plate to investigate the detailed seismic structure in the mantle wedge beneath the south Kyushu area, Japan. Our results show a trench-normal (subduction-parallel) anisotropy that lies just beneath the volcanic arc. We discuss a cause of the newly found seismic anisotropy in terms of a slip system of mantle minerals, especially C-type of olivine, and relate it to the distribution of fluid in the mantle wedge beneath the south Kyushu area.

2. Data and methods

We use seismic waveform data recorded with sampling frequency of 100 Hz at Hi-net stations operated by the National Research Institute for Earth Science and Disaster Prevention (NIED) in the south Kyushu area, Japan. The period of the analysis covers the years of 2004–2010 (Figure 2). This period is different from that, the years of 2000-2006, of a previous work of *Salah et al.* [2009] in this area, providing a new data set of shear wave splitting.

We analyze waveform data that satisfy the following conditions. Source depths are restricted to those greater than 30 km to investigate seismic anisotropy in the mantle wedge. Incident angles are less than 35° to minimize the effect of phase conversion from S to P or distortion of particle motions at the free surface [*Booth and Crampin*, 1985]. The hypocenter catalogue reported by Japan Meteorological Agency and a three-dimensional velocity structure of *Matsubara et al.* [2008] and *Matsubara and Obara* [2011] are used to estimate the incident angle to the stations (Figure 1). We calculate the ray paths that are propagated through the three-dimensional heterogeneous V_S structure.

We estimate the splitting parameters φ and δt using the covariance matrix decomposition method of *Silver and Chan* [1991] from the two band-pass filtered (1–20 Hz) horizontal components of S waves (Figure 3). We search for the optimum pair (φ, δt) that minimizes the eigenvalue of the covariance matrix in the ranges of 0° to 180° with an increment of 1° for φ and of 0 to 1 s with an increment of 0.01 s for δt. The errors of φ and δt are estimated using the method of *Silver and Chan* [1991]. We also confirm visually that the obtained splitting parameters are coincident with the initial motion of S waves from the particle motion. This procedure is important to assure the validity of the splitting analysis. A lack of this procedure may cause apparent variation in splitting parameters.

The waveforms we analyze here are typically lack higher frequencies because of seismic attenuation in the mantle wedge. We apply the band-pass filter not only to enhance the S/N ratio of the waveforms but also to make the initial motion of S waves clear because it is difficult for reconstructed waveforms with only lower frequencies to estimate the initial motion of S waves from the particle motion.

3. Results

We obtain a total of 65 shear wave splitting measurements at eight stations from 392 events in the south Kyushu area (Figures 2 and 4). The observed φ and δt respectively show NEE–SWW to NWW–SEE and 0.04–0.63 s. The estimated errors of φ and δt respectively are usually less than 10° and 0.02 s. These results of φ and δt are roughly coincident with those in the south Kyushu area reported by *Salah et al.* [2009], in which the dominant φ is close not to trench-parallel but to trench-normal, although our results show a smaller variation than those of *Salah et al.* [2009]. In several subduction zones, a difference in the polarization direction exists between the forearc region and the backarc region. For example, *Nakajima and Hasegawa* [2004] reported that trench-parallel polarization is observed in the forearc region and trench-normal one in the backarc region in the NE Japan. We, however, observe no distinct spatial variation in the polarization direction between the forearc and the backarc regions in the south Kyushu area.

Long and van der Hilst [2006] claimed that the average polarization in this area is trench-parallel based on longer period data than those in this study: two frequency ranges of 0.02–0.125 Hz and 0.1–1 Hz, although their data includes some distinct trench-normal polarizations and oblique ones. It is possible to compare the splitting results of *Long and van der Hilst* [2006], *Salah et al.* [2009] and this study directly

within south Kyushu. The results of *Salah et al.* [2009] (Figure 14 in their paper) are coincident with our results. *Salah et al.* [2009] showed that the dominant polarization direction φ is NW-SE at a broadband F-net station TKA operated by NIED although minor amount of NE-SW trending polarization are observed. The TKA results of *Long and van der Hilst* [2006] are not coincident with them (Figure 4 in their paper). In either case, it is obvious that the results do not support trench-parallel polarization in the south Kyushu.

In this study, we have rejected most of the results of shear wave splitting for which we could not recognize the consistency between the polarization direction from waveform analysis and that from the particle motion. Some of the examples shown in the previous papers seem not to satisfy our criteria. In conclusion, the difference from descriptions of the previous studies is mainly due to sampling bias and different extents of waveform examination. We argue that trench-parallel polarization as an averaged result of small number of data with a large variation cannot represent accurately a structure beneath the south Kyushu area.

If we note the delay time, we can find a difference between the forearc and backarc regions. We observe larger delay times up to 0.63 s in the backarc region, although smaller delay times up to 0.15 s are observed in the forearc region in this study.

Shear wave splitting of which the delay time is less than 0.3 s is possibly induced by crustal anisotropy because the crustal anisotropy produces delay times of up to 0.3 s [*e.g., Kaneshima*, 1990; *Savage*, 1999]. Furthermore, shear wave splitting from the crustal anisotropy is usually coincident with the regional maximum horizontal compressional stress [*Kaneshima*, 1990]. In fact, we recognize clearly that the polarization direction of which the delay time is less than 0.3 s is coincident with the orientation of a regional maximum horizontal compressional stress [*Ishise and Oda*, 2009] (Figure 5). The observed shear wave splitting of which the delay time is less than 0.3 s is therefore caused probably not by the mantle anisotropy but by the crustal anisotropy in this region. We therefore use the results for which the delay time is greater than 0.3 for discussion of a cause of the seismic anisotropy in the mantle wedge beneath the south Kyushu area.

Figure 4b shows ray paths and the V_P/V_S structure [*Matsubara et al.,* 2008; *Matsubara and Obara, 2011*] on the cross section along the profile A–B in Figure 4a. Many ray paths have delay time greater than 0.3 s for the shear waves through the high V_P/V_S region at the depth of 100–150 km beneath the volcanic front in the mantle wedge. Not only are the shear waves with delay times are greater than 0.3 s but also those for which delay times are less than 0.3 s pass through the shallower mantle beneath the

stations, indicating that the shallower mantle is less anisotropic. We therefore consider

that the anisotropic region is localized in the high V_P/V_S region at a depth of 100–150

km beneath the volcanic front in the south Kyushu area.

4. Possible causes of trench-normal anisotropy

The previous S-wave analyses using teleseismic and local events detected

trench-parallel alignments of faster shear wave polarizations on average in the Ryukyu

arc including the south Kyushu area [*Long and van der Hilst,* 2005; 2006]. *Long and*

van der Hilst [2006] also emphasized that a minor but meaningful share of

trench-normal polarizations are detected and they are mostly sampling the backarc side

mantle. For this study, we used seismic waves propagating at a high angle against the

subduction boundary to detect the mantle structure affected by the downgoing slab. The

results constrain the exact locality of the anisotropy with the trench-normal

(subduction-parallel) polarization beneath the south Kyushu area: large delay times

observed for deeper events below 125 km for which ray paths run across the high V_P/V_S

region at depths of 100–150 km; small delay times for the shallower events constrain

the depth of the anisotropic region as greater than 100 km (Figure 4). The location of

the anisotropic region implies that the characteristics of the mantle might be related to the volcanic front immediately above.

Orientations of mantle wedge anisotropy are generally discussed based on preferred orientation of elastically anisotropic minerals such as olivine [*Jung and Karato*, 2001; *Nakajima and Hasegawa*, 2004; *Jung et al.*, 2006; *Long and van der Hilst*, 2006] and antigorite [*Park et al.*, 2004; *Nikulin et al.*, 2009; *Katayama et al.*, 2009; *Bezacier et al.*, 2010; *Mookherjee and Capitani*, 2011]. The stability of these minerals in the mantle wedge can be inferred from subduction geotherms. However, model calculations for the thermal states are affected strongly by many factors such as initial geotherm, mantle flow, and age of subducting plate [*Yoshioka et al.*, 2008; *Peacock*, 2009; *Syracuse et al.*, 2010]. In the case of the south Kyushu area, the subducting Philippine Sea plate comprises 55–35 Ma oceanic plate and remnants of paleo-arcs (i.e., Kyushu-Palau Ridge, Amami Plateau and Daito Ridge) [*Hilde and Lee*, 1984; *Okino et al.*, 1994; *Deschamps and Lallemand*, 2002; *Haraguchi et al.*, 2003; *Hickey-Vargas*, 2005; *Ishizuka et al.*, 2011]. The plate ages are intermediate of the Philippine Sea slab subducting beneath Shikoku and the Pacific slab beneath the NE Japan. However, the existence of the old arcs probably causes significant variation in the thermal structure of the subducting plate. Considering subduction of the old arc

lithosphere like the Amami Plateau with the Ar–Ar ages of 95–116 Ma [*Hickey-Vargas*, 2005], the possible coldest estimation can be close to the geotherm under the NE Japan along which antigorite is stable at depths of 100–150 km [*Peacock and Wang*, 1999; *Syracuse et al.*, 2010].

To identify the cause of shear wave polarization anisotropy in the mantle wedge beneath the south Kyushu area, we compare the observations with theoretical shear wave splittings calculated from elastic constants of mantle minerals. For simplicity, we assume olivine or serpentine as a dominant phase that causes seismic anisotropy in the mantle wedge. To model polycrystalline rocks, we used a mixture of a synthesized random fabric and an oriented single crystal of olivine or antigorite. An ab-initio calculation for equation of state of antigorite suggests that the strength of quasi-hexagonal anisotropy of antigorite is expected not to change greatly at pressures of 1–5 GPa (AVs = 50–60%) [*Mookherjee and Capitani*, 2011] and that the strength of anisotropy at high pressures closely resembles experimentally obtained results at ambient pressure and temperature [*Bezacier et al.*, 2010]. Therefore, we use the experimentally determined elastic constants of antigorite for discussions on the strength of anisotropy in the mantle wedge (Table 1). Olivine elastic constants are referred to *Abramson et al.* [1997] (Table 1).

Dominant slip systems in olivine and resultant CPOs are known to change with P–T conditions and water contents [*Jung et al.,* 2006; *Karato et al.,* 2008]. Our model calculation tests four patterns of orientation of olivine crystal corresponding to the A-type, B-type, C-type, and E-type CPOs. For a reference frame, we defined the X1 axis to be parallel to the dip angle of the Philippine Sea plate, the X2 axis to be parallel to the strike, and the X3 axis to be normal to the slab surface (Figure 6), which assumes a subduction-parallel flow in the mantle wedge. The combination of the X1, X2, and X3 axes and olivine *a*, *b*, and *c* axes are presented in Table 3. For antigorite, we set the *a*-axis as the X1 axis, the *b*-axis as the X2 axis and the *c*-axis as the X3 axis. This pattern of antigorite CPO is confirmed in experimental samples that have been recrystallized under shear deformation [*Katayama et al.,* 2009] and it is also found in natural serpentinites [*Bezacier et al.,* 2010; *Padrón-Navarta et al.,* 2012]. The mechanism for the CPO is interpreted as dislocation gliding with a [100](001) slip system [*Katayama et al.,* 2009; *Padrón-Navarta et al.,* 2012]. Some researchers reported natural evidence for a different type of antigorite CPO, in which the *b*-axes, instead of the *a*-axes, align parallel to the stretching lineation [*Soda and Takagi,* 2010; *Hirauchi et al.,* 2010; *Jung,* 2011; *Nishii et al.,* 2011]. The reason for the formation of these different types of patterns is unclear. Seismic properties parallel to the *a*- and

b-axes of antigorite are very similar and so the degree to which the *a*- and *b*-axes are aligned parallel to the lineation has little effect on the predicted seismic properties. Based on seismic observations of the Philippine Sea slab configuration [*Hirose et al.*, 2008; *Nakajima and Hasegawa*, 2007], we assume the dip angle of 60° from the horizontal plane and the strike of 80° from north to west as a geometry of a deeper part of the subducting PHS slab beneath the south Kyushu area.

We calculate the polarization direction and the velocity of quasi-S waves using the Christoffel equations as

$$(C_{ijkl}X_jX_l - \delta_{ik}\rho V^2)\, g_k = 0, \qquad (1)$$

where C_{ijkl}, X_j, δ_{ik}, ρ, V, and g_k respectively denote the elastic constants, the vector showing the propagation direction of seismic wave, Kronecker's delta, the density, the seismic velocity and the vector showing a polarization direction of seismic wave. The Einstein summation convention is applied to all repeated lower indices, which take values of 1, 2, and 3. We also apply the tensor transformation law to coincide the frame of the crystal with the geographical frame in the calculation. The propagation direction of the shear wave used in the calculation is estimated at the slab surface for each ray path. However, it is noteworthy that a strong tradeoff exists between the anisotropic layer thickness and the degree of CPO. That is, the thickness and the degree portrayed

in Figure 7 are not unique ones but represent one of the possible combinations that match the observed delay times. We, thereby, specifically examine the polarization direction in this calculation.

We show that the results of synthesized shear wave splitting in Figure 7 present a comparison with the observed one at two stations: N.KORH and N.MYJH. Data from these stations show clear and internally consistent shear wave polarizations with delay times greater than 0.3 s. In Figure 7, the C-type olivine fabric with the trench-parallel *b*-axis and the trench-normal *c*-axis dipping 60°W agrees well with the observed anisotropy. The theoretically calculated polarization directions based on the B-type olivine are trench-parallel (Figure 7b) and are almost perpendicular to the observed ones. For the case of the A-type, the discrepancy between the theoretical and observed ones is as large as 40°. The results for the E-type are close but still oblique, the discrepancy as large as 20°, to the observed polarizations. Serpentinite with a strong schistosity parallel to the subduction boundary produces a trench-parallel fast polarization as suggested by *Katayama et al.* [2009] and normal to the observed polarization direction. Therefore, the results of our calculation show that C-type olivine CPO is the most likely cause of the seismic anisotropy beneath the volcanic front in the south Kyushu. Recently Wirth and Long (2012) ruled out both serpentine and olivine B-fabric in the anisotropic layer

above the subducting Pacific plate beneath NE Honshu, Japan, from receiver function

analyses because their inferred anisotropic fast axis is parallel or oblique to the dip of

the downgoing slab.

We discuss the relation between the polarization directions and the type of CPO

and show that the C-type olivine is the most plausible to date. We specifically address

the delay times and the strength of anisotropy or the thickness of anisotropic layer.

Frese et al. [2003] reported the natural examples of the C-type olivine CPO from Cima

di Gagnone, central Alps, and estimated the strength of anisotropy using CPOs of the

constituent minerals and the modal proportions. We apply the strength of anisotropy

reported by *Frese et al.* [2003], 1.4–2.4%, to the splitting times observed in the south

Kyushu area for the estimation of the layer thickness. Sampling of crustal anisotropy, up

to 0.3 s, is considered [*Kaneshima*, 1990], providing the contribution of the mantle

anisotropy is around 0.3 s and greater because the observed polarization directions are

similar for the crustal and the mantle anisotropy. Figure 8 shows a relation between the

anisotropic layer thickness and the delay time based on results reported by *Frese et al.*

[2003]. The result to produce the delay time of 0.3 s is 30–100 km of thickness,

reflecting variation in the CPO strength of the peridotite. These first-order estimations

of layer thickness are comparable to the thickness of the high V_P/V_S region, ca. 50 km,

as depicted by seismic tomography [*Matsubara et al.*, 2008; *Matsubara and Obara*, 2011].

Deformational experiments at pressures of 2–3 GPa show that the C-type CPO can be formed at higher temperatures and/or lower stress [*Jung and Karato*, 2001; *Jung et al.*, 2006; *Katayama and Karato*, 2006]. Recent experimental studies are assessed to examine the distribution of the olivine fabric at depths greater than 100 km. *Couvy et al.* [2004] conducted multi-anvil deformational experiments using wet polycrystalline olivine samples. They found weak development of C-type olivine CPOs at 11 GPa with dislocation structures of a [001] slip. A D-DIA experiment under higher pressures (approx. 5.2 GPa) revealed that a higher water content in olivine (above 650 ppm H/Si) enhances the stability of the B-type with respect to the A-type [*Ohuchi et al.*, 2012]. They suggested that the C-type olivine fabric is less dominant up to water content of 1700 ppm H/Si. However, *Shekhar* [2012] showed that the [001] slip on (100) producing the C-type CPO becomes dominant in more water-rich olivine (1500–7500 ppm H/Si) under pressures of 3.0–8.5 GPa.

Our seismic observations of the trench-normal anisotropy are clearly inconsistent with the B-type CPO. The C-type is the best fit. Considering the coincidence with the high V_P/V_S ratio, low V_P and low V_S [*Matsubara et al.*, 2008;

Matsubara and Obara, 2011] (Figure 4), we infer that the anisotropy represents extensive development of the C-type fabric in extremely H_2O-rich mantle. *Nakajima and Hasegawa* [2004] reported that the trench-normal anisotropy at the western side of the NE Japan results from the A-type olivine CPO dominated by [100](010) slip system at high temperature and dry conditions [*Nicolas and Christensen*, 1989; *Karato et al.*, 2008]. Our results of seismic anisotropy for the south Kyushu area indicate that such dry conditions are not necessary for trench normal anisotropy in a mantle wedge.

5. Subduction fluid transport beneath south Kyushu

A question arising here is why such high water activity is achieved in this region. It is probably related to both a supply of aqueous fluid from the subducting plate and mobility of such fluid in the mantle wedge. The stability of hydrous minerals is regarded as a major control for depths and extents of fluid releases from slabs. It depends on pressure–temperature curves along subduction boundaries [*Schmidt and Poli*, 1998; *Poli and Schmidt*, 2002; *Hacker et al.*, 2003]. *Mibe et al.* [1999] proposed that the dihedral angle between olivine grains and interstitial fluid is a function of pressure and temperature and that it can be a controlling factor of fluid mobility in

mantle wedge. Herein, we briefly discuss the P–T conditions expected along the south

Kyushu subduction boundary and consider likely mechanisms to bring water to the

mantle.

Our seismic analyses and model calculations indicate that antigorite

serpentinite is probably not stable at depths over 100 km as the C-type olivine fabric is

most likely for the anisotropic region at the depth. In order to make the olivine fabric

dominant at depth, the south Kyushu subduction geotherm must intersect with the

univariant curve of antigorite stability at about 650°C and 3 GPa (Figure 9). This

seismologically constrained geotherm is the coldest estimation and it is rather close to

those beneath Shikoku rather than those beneath NE Japan. The higher limit of the

subduction zone thermal gradient is constrained by the absence of geological evidence

for slab melting. The thermal conditions of the subducting slab do not exceed the

melting temperatures of MORB under wet conditions [*Schmidt and Poli*, 1998]. The

tomographic image of the south Kyushu section shows that the high V_P/V_S region

extends in thickness of, at least, 40 km from the surface of the subducting slab

[*Matsubara et al.*, 2008; *Matsubara and Obara*, 2011] (Figure 1b). The thermal

modeling of Peacock and Wang [1999], that assumed a relatively weak coupling

between mantle wedge and subducting slab, suggests that temperature conditions in

mantle wedge at 40 km above subduction surfaces are 1000-1100°C at depths of 100-150 km. They are significantly cooler than melting temperatures of mantle in wet conditions at the relevant pressures [*Green et al.*, 2010]. This is consistent with our interpretation that the C-type olivine fabric has developed through ductile deformation under water-rich conditions.

Using this range of geotherm along the subduction boundary, we can roughly estimate the depths at which major hydrous minerals in the Philippine Sea slab (assuming basaltic compositions) are broken down: lawsonite to zoisite (60–80 km), amphibole to cpx (80 km), and zoisite to garnet + cpx (100 km) [*Schmidt and Poli*, 1998] (Figure 9). Our estimation indicates that the basaltic slab might mostly consist of anhydrous minerals at the depths of the anisotropic region. Exceptionally, the coolest estimate of the south Kyushu geotherm, allows for the existence of lawsonite at those depths (Figure 9). However, lawsonite would not behave as a carrier of water but as an acceptor along this geotherm. Consequently, it can be considered that the major release of water-rich fluid from the basaltic slab takes place at depths of 60-100 km. On the other hand, the inferred geotherm intersects with high temperature limit of antigorite stability, which depends on chemical compositions of antigorite [*Bromiley and Pawley,* 2003], at the depth of about 100-120 km. This allows that antigorite is developed in the

mantle wedge just above the slab and that antigorite can behave as a carrier of water

expelled out from dehydration reactions in the basaltic slab down to the depth of

100-120 km. Furthermore, it is also expected that chlorite can partly take over the water

in antigorite (up to 60%) in the deeper mantle [*Hacker et al.*, 2003]. The petrological

transportation of water can be a mechanism to cause the high V_P/V_S region beneath

south Kyushu. However, we have no seismological observation indicating extensive

serpentinization near the subduction boundary, especially at depths of 60–100 km. This

makes us hesitate to attribute the water transport to the 150 km depth to hanging wall

serpentinite.

It is more likely that antigorite serpentinite in the subducting slab contributes to

a connection of the missing link to the subduction zone below 100 km depth because

slab Moho is cooler than the subduction surface [*Peacock and Wang*, 1999; *Yoshioka et

al.*, 2008]. The remnant arcs on the subducting Philippine Sea plate might be associated

with major faults cross-cutting the lithosphere. *Ueda et al.* [2011] described

development of 5-km-thick serpentinite underlying the Paleogene volcaniclastics of the

Izu-Bonin-Mariana arc. They related the serpentinite structure to a large fracture zone

(SofuganTectonic Line) or the N–S extension of remnant arcs in the Philippine Sea plate.

The development of a high V_P/V_S region in the south Kyushu subducting slab (Figure

1b) [*Matsubara et al.,* 2008; *Matsubara and Obara,* 2011] and the high density of earthquake hypocenters at depths of 100–150 km (Figure 2) are consistent with the existence of fluid in the slab. *Faccenda et al.* [2008] suggested that the main anisotropic sources of SKS waves in the circum Pacific subduction zones lie within subducting slabs. They attributed the anisotropy to trench-parallel fluid or antigorite-filled fractures that have been formed due to plate bending at outer rises and trench slopes. *Sumino et al.* [2010] showed natural evidence that seawater can penetrate downward to 100 km depth in a subduction setting as pore fluids maintaining the halogen isotope signature near the sea floor. The above geophysical and geochemical evidences support extensive hydration of oceanic mantle. However, more detailed investigations must be undertaken to discuss the distribution and the likely causes in the Philippine Sea slab under the south Kyushu arc.

To attain a wide distribution of the C-type olivine fabric in the mantle wedge, water must be kept in the mantle under deformation. *Mibe et al.* [1999] showed that the dihedral angle of the fluid–olivine interface varies with pressure and temperature. This can be a major control of fluid mobility. If the angle is greater than 60°, then the fluids in interstitial space are isolated and tend to remain. However, if the angle is smaller than 60°, then the interstitial space of olivine grains filled by fluids will be connected to

make pathways through which the fluids can flow. We compare the temperature structure on the slab surface beneath the south Kyushu area with the isodepth of the dihedral angle at 60° in P–T space (Figure 9). We also indicate the high V_P/V_S region as the anisotropic region in this diagram. The anisotropy is mainly developed in the P–T conditions where the dihedral angle is larger than 60°, showing that the fluid mobility is limited at depths shallower than 150 km. It is noted that this estimation is associated with a significant error as about 10–20 km because of a large uncertainty in the inferred geotherm.

Our seismological observations indicate the existence of water-saturated mantle with trench-normal anisotropy just below the volcanic front at the south Kyushu. We can presume the genetic relation between the water-rich mantle at depths and the explosive volcanism at the surface [*Aramaki*, 1984; *Machida*, 1999] although we don't have sufficient geophysical information on the shallow mantle that directly relates the tectonic and petrological events with the deep mantle.

As stated above, the seismologically constrained geotherm proposed in this paper allows, in terms of thermal conditions, the development of serpenitinite in the forearc mantle. However, we observed no significant shear wave splitting from the mantle wedge of the forearc region shallower than 100 km. In the central and southern

part of the Ryukyu arc, strong trench-parallel fast polarization (delay time of 2 s) observed in deeper origins of local events and no strong anisotropy is also detected at the shallowest mantle [*Long and van der Hilst*, 2006]. The maximum delay times of 0.3 s for the shallow ray paths in south Kyushu are comparable to those caused by the crustal anisotropy [*Kaneshima*, 1990]. A fully serpentinized layer with a thickness of 3 km can cause a delay time of 0.3 s [*Hilairet and Reynard,* 2009; *Bezacier et al.*, 2010]. If a serpentine layer exists there, then it might be too thin to cause observable shear wave splitting. *Hilairet and Reynard* [2009] reported that the serpentinite layer thickness must be thin (not exceeding 3 km) to keep serpentinite subduction channel in which thinning (shrinkage) attributable to buoyant upward flow and thickening, kinetically controlled by serpentinization, are competing. *Nikulin et al.* [2009] proposed a similar idea based on receiver function analyses in the Cascadia subduction zone that antigorite serpentinite has been expelled upward along the subduction boundary to form an anisotropic low-velocity sliver with a thickness of 7-10 km just beneath the continental crust.

6. Conclusions

Seismic anisotropy in the mantle wedge beneath the south Kyushu area, Japan, was examined by shear wave splitting from local intermediate-depth earthquakes. The direction of the faster polarization of shear wave is normal to the trench (parallel to the plate subduction). Results of splitting analyses using various ray paths covering the mantle wedge suggest that the spatial distribution of the anisotropic region is probably coincident with a high V_P/V_S region at the depth of 100–150 km beneath the volcanic front of the Ryukyu arc. The model calculation of splitting parameters shows that the C-type olivine CPO with the trench-parallel b-axis and the trench normal c-axis inclined 60° from the horizontal explain the observations well. The inferred strength of the anisotropy applying the thickness of the high V_P/V_S region is comparable to that of natural examples from Alpe Arami. These results suggest the existence of fluid in this region. Concentration of interstitial fluid in peridotite might be controlled by high dihedral angles among olivine–fluid interfaces at depths greater than 150 km. The development of the C-type olivine fabric at 100 km depth puts a constraint on the thermal conditions along the subduction boundary, implying that the hydrous minerals in the basaltic slab are mostly broken down at the shallower depths. Therefore, the carrier of water in the south Kyushu subduction zone probably lies in the slab mantle, the most likely is serpentinized oceanic lithosphere. Our results suggest a relation

between the wet mantle immediately above the subducting slab and the explosive

magma activities in the south Kyushu area. More detailed geophysical investigations

must be conducted to examine the shallow structures to elucidate the whole system of

material circulation that results in huge volcanic disasters.

Acknowledgments

References

Abramson, E. H., J. M. Brown, L. J. Slutsky, and J. Zaug (1997), The elastic constants

of San Carlos olivine to 17 GPa, *J. Geophys. Res.*, *102*, 12253–12263.

Ando, M., Y. Ishikawa, and H. Wada (1980), S-wave anisotropy in the upper mantle under a volcanic area in Japan, *Nature*, *268*, 43–46.

Aramaki, S. (1984), Formation of the Aira Caldera, southern Kyushu, <22,000 years ago, *J. Geophys. Res.*, *89*, 8485–8501.

Bezacier, L., B. Reynard, J. D. Bass, C. Sanchez-Valle, and B. Van de Moortèle (2010), Elasticity of antigorite, seismic detection of serpentinites and anisotropy in subduction zones, *Earth Planet. Sci. Lett.*, *289*, 198–208.

Booth, D. C., and S. Crampin (1985), Shear-wave polarizations on a curved wave-front at anisotropic free surface, *Geophys. J. R. Astron. Soc.*, *83*, 31–45.

Bromley, G. D., and A. R. Pawley (2003), The stability of antigorite in the systems $MgO-SiO_2-H_2O$ (MSH) and $MgO-Al_2O_3-SiO_2-H_2O$ (MASH): the effects of Al^{3+} substitution on high-pressure stability, *American Mineralogist*, *88*, 99–108.

Couvy, H., Frost, D. J., Heidelbach, F., Nyilas, K., Ungár, T., Mackwell, S., and Cordier, P. (2004), Shear deformation experiments of forsterite at 11 GPa – 1400 ºC in the multianvil apparatus, *Eur. J. Mineral.*, *16*, 877–889.

Deschamps, A., and S. Lallemand (2002), The West Philippine Basin: An Eocene to early Oligocene back arc basin opened between two opposed subduction zones, *J. Geophys. Res.*, *107*, 2322, doi:10.1029/2001JB001706

Faccenda, M., L. Burlini, T. V. Gerya, and D. Mainprice (2008), Fault-induced seismic

anisotropy by hydration in subducting oceanic plates, *Nature*, *455*, 1097–1100.

Frese, K., V. Trommsdorff, and K. Kunze (2003), Olivine [100] normal to foliation:

lattice preferred orientation in prograde garnet peridotite formed at high H_2O

activity, Cima di Gagnone (Central Alps), *Contrib. Mineral Petrol.*, *145*, 75–86.

Green, D. H. (1973), Experimental melting studies on a model upper mantle

composition at high pressures under water-saturated and water-undersaturated

conditions, *Earth Planet. Sci. Lett.*, *19*, 37–53.

Greve, S. M., M. K. Savage, and S. D. Hofmann (2008), Strong variations in seismic

anisotropy across the Hikurangi subduction zone, North Island, New Zealand,

Tectonophys., *462*, 7-21.

Grove, T. L., C. B. Till, E. Lev, N. Chatterjee, and E. Medard (2009), Kinematic

variables and water transport control the formation and location of arc volcanoes,

Nature, *459*, 694–697.

Hacker, B. R., G. A. Abers, and S. M. Peacock (2003), Subduction factory 1.

Theoretical mineralogy, densities, seismic wave speeds, and H_2O contents, *J.

Geophys. Res.*, *108*, doi:10.1029/2001JB001127,

Haraguchi S., T. Ishii, J.-I. Kimura, and Y. Ohara (2003), Tonalite from basaltic magma

at the Komahashi–Daini Seamount, northern Kyushu–Palau Ridge in the Philippine Sea, and growth of the Izu–Ogasawara (Bonin)–Mariana arc crust, *Contrib. Mineral. Petrol.*, *145*, 151–168.

Hikey-Vargas, R. (2005) Basalt and tonalite from the Amami Plateau, northern West Philippine Basin: New Early Cretaceous ages and geochemical results, and their petrologic and tectonic implications, *The Island Arc*, *14*, 653–665.

Hilairet, N., and B. Reynard (2009), Stability and dynamics of serpentinite layer in subduction zone, *Tectonophysics*, *465*, 24–29.

Hilde T. W. C., and C. -S. Lee (1984), Origin and evolution of the West Philippine Basin: A new interpretation, *Tectonophysics, 102*, 85–104.

Hiramatsu, Y., M. Ando, T. Tsukuda, and F. Ooida (1998), Three-dimensional image of the anisotropic bodies beneath central Honshu, Japan, *Geophys. J. Int.*, *135*, 801–816.

Hirauchi, K., K.Michibayashi, H. Ueda, and I. Katayama (2010), Spatial variations in antigorite fabric across a serpentinite subduction channel : Insights from the Ohmachi Seamount, Izu-Bonin frontal arc, *Earth Planet. Sci. Lett.*, *299*, 196-206.

Hirose, F., J. Nakajima, and A. Hasegawa (2008), Three-dimensional seismic velocity structure and configuration of the Philippine Sea slab in southwestern Japan

estimated by double-difference tomography, *J. Geophys. Res.*, *113*, B09315, doi:10.1029/2007JB005274.

Hyndman, R. D. and S. M. Peacock (2003), Serpentinization of the forearc mantle, *Earth Planet. Sci. Lett.*, *212*, 417–432.

Ishise, M and H. Oda (2009), Anisotropic Velocity Structure of Seismic Waves in Japan Subduction Zone, *J. Seismo. Soc. Jpn*, *61*, 187–197 (in Japanese with English abstract).

Ishizuka, O., R. N. Taylor, M. Yuasa, and Y. Ohara (2011), Making and breaking an island arc: A new perspective from the Oligocene Kyushu-Palau arc, Philippine Sea, *Geochem. Geophys. Geosyst.*, *12*, Q05005, doi:10.1029/2010GC003440.

Jung, H. (2011), Seismic anisotropy produced by serpentine in mantle wedge, *Earth Planet. Sci. Lett.*, *307*, 535-543.

Jung, H. and S. Karato (2001), Water-induced fabric transitions in olivine, *Science*, *293*, 1460–1463.

Jung, H., I. Katayama, Z. Jiang, T. Hiraga, and S. Karato (2006), Effect of water and stress on the lattice preferred orientation of olivine, *Tectonophys.*, *421*, 1–22.

Kaneshima, S. (1990), Origin of crustal anisotropy: Shear Wave splitting studies in Japan, *J. Geophys. Res.*, *95*, 11121–11133.

Karato, S., H. Jung, I. Katayama, and P. Skemer (2008), Geodynamic significance of

seismic anisotropy of the upper mantle: New insights from laboratory studies, *Annu.*

Rev. Earth Planet. Sci., *36*, 59–95.

Katayama, I., K. Hirauchi, K. Michibayashi, and J. Ando (2009), Trench-parallel

anisotropy produced by serpentine deformation in the hydrated mantle wedge,

Nature, *461*, 1114–1117.

Katayama, I., and S. Karato (2006), Effect of temperature on the B- to C- type olivine

fabric transition and implication for flow pattern in subduction zones, *Phys. Earth*

Planet. Int., *157*, 33–45.

Levin, V., D. Droznin, J. Park, and E. Gordeev (2004), Detailed mapping of seismic

anisotropy with local shear waves in southeastern Kamchatka, *Geophys. J. Int.*, *158***,**

1009–1023.

Long, M. D. and P. G. Silver (2009), Mantle flow in subduction systems: the subslab

flow field and implications for mantle dynamics, *J. Geophys. Res.*, *114*, B10312,

doi:10.1029/ 2008JB006200.

Long, M. D., and R. D. van der Hilst (2005), Upper mantle anisotropy beneath Japan

from shear wave splitting, *Phys. Earth Planet. Inter.*, *151*, 206–222.

Long, M. D., and R .D. van der Hilst (2006), Shear wave splitting from local events

beneath the Ryukyu arc: Trench-parallel anisotropy in the mantle wedge, *Phys.*

Earth Planet. Inter., *155*, 300–312.

Machida, H. (1999), The stratigraphy, chronology and distribution of distal

marker-tephras in and around Japan, *Global and Planetary Change*, *21*, 71–94.

Matsubara, M., K. Obara, and K. Kasahara (2008), Three-dimensional P-and S-wave

velocity structures beneath the Japan Islands obtained by high-density seismic

stations by seismic tomography, *Tectonophysics*, *454*, 86–103.

Matsubara, M. and K. Obara (2011), The 2011 Off the Pacific Coast of Tohoku

earthquake related to a strong velocity gradient with the Pacific plate, *Earth Planets*

Space, *63*, 663–667.

Mibe, K., T. Fujii, and A. Yasuda (1999), Control of the location of the volcanic front in

island arcs by aqueous fluid connectivity in the mantle wedge, *Nature*, *401*, 259–

262.

Mookherjee, M., and G. C. Capitani (2011), Trench parallel anisotropy and large delay

times: Elasticity and anisotropy of antigorite at high pressures, *Geophys. Res. Lett.*,

38, L09315, doi:10.1029/2011GL047160.

Nakajima, J. and A. Hasegawa (2004), Shear-wave polarization anisotropy and

subduction induced-flow in the mantle wedge of northeastern Japan, *Earth Planet.*

Sci. Lett., *225*, 365–377.

Nakajima, J., and A. Hasegawa (2007), Subduction of the Philippine Sea plate beneath

southwestern Japan: Slab geometry and its relationship to arc magmatism, *J.*

Geophys. Res., *112*, B08306, doi:10.1029/2006JB004770.

Nicolas, A. and N. I. Christensen (1987), Formation of anisotropy in upper mantle

peridotites -a review. In *Composition, Structure and Dynamics of the*

Lithosphere-Asthenosphere System (K. Fuchs and C. Froideoaux, eds.), pp. 111–

123, AGU, Washington, D. C.

Nikulin, A., V. Levin, and J. Park (2009), Receiver function study of the Cascadia

megathrust: Evidence for localized serpentinization, *Geochem. Geophys. Geosyst.*,

10, Q07004, doi:10.1029/2009GC002376.

Niida, K., and D. H. Green (1999), Stability and chemical composition of pargastic

amphibole in MORB pyrolite under upper mantle conditions, *Contrib. Mineral.*

Petrol., *135*, 18–40.

Nishii, A., S.R. Wallis, T. Mizukami, and K. Michibayashi (2011), Subduction related

antigorite CPO patterns from forearc mantle in the Sanbagawa belt, southwest

Japan, *J. Struct. Geol.*, *33*, 1436-1445.

Ohuchi, T., T. Kawazoe, Y. Nishihara, and T. Irifune (2012), Change of olivine a-axis

alignment induced by water: Origin of seismic anisotropy in subduction zones, *Earth Planet. Sci. Lett.*, *317–318*, 111–119.

Okino, K., Y. Shimakawa, and S. Nagaoka (1994), Evolution of the Shikoku basin, *J. Geomag. Geoelectr.*, *46*, 463–479.

Padrón-Navarta, J. A., A. Tommasi, C. J.Garrido, and V. L. Sánchez-Vizcaíno (2012), Plastic deformation and development of antigorite crystal preferred orientation in high-pressure serpentinites, *Earth Planet. Sci. Lett.*, *349–350*, 75–86.

Park, J., H. Yuan, and V. Levin (2004), Subduction-zone anisotropy under Corvallis, Oregon: A serpentinite skidmark of trench-parallel terrane migration?, *J. Geophys. Res.*, *109*, B10306, doi:10.1029/2003JB002718.

Peacock, S. M., and K. Wang (1999), Seismic consequences of warm versus cool subduction metamorphism: examples from southwest and northeast Japan, *Science*, *286*, 937–939.

Peacock, S. M. (2009), Thermal and metamorphic environment of subduction zone episodic tremor and slip, *J. Geophys. Res.*, *114*, B00A07, doi:10.1029/2008JB005978.

Poli, S., and M. W. Schmidt (2002), Petrology of subducted slabs, *Annu. Rev. Earth*

Planet. Sci., *30*, 207–235.

Russo, R .M., and P. G. Silver, (1994), Trench-parallel flow beneath the Nazca plate

from seismic Anisotropy, *Science*, *263*, 1105–1111.

Salah, M.K., T. Seno, and T. Iidaka (2009), Seismic anisotropy in the wedge above the

Philippine Sea slab beneath Kanto and southwest Japan derived from shear wave

splitting, *J. Asian Earth Sci.*, *34*, 61-75.

Savage, M. K. (1999), Seismic anisotropy and mantle deformation: What have we

learned from shear wave splitting?, *Reviews of Geophysics*, *37*, 65–106.

Schmidt, M. W., and S. Poli (1998), Experimentally based water budgets for

dehydrating slabs and consequences for arc magma generation, *Earth Planet. Sci.*

Let., *163*, 361–379.

Shekhar, S. (2012), The origins of olivine fabric transitions and their effects on seismic

anisotropy in the upper mantle, PhD thesis, University of Bayreuth,

http://opus4.kobv.de/opus4-ubbayreuth/frontdoor/index/index/docId/1063.

Silver, P. G. and W. W. Chan (1991), Shear wave splitting and subcontinental mantle

deformation, *J. Geophys. Res.*, *96*, 16429–16454.

Soda, Y. and H. Takagi (2010), Sequential deformation from serpentinite mylonite to

metasomatic rocks along the Sashu Fault, SW Japan, *J. Struct. Geol.*, *32*, 792-802.

Sumino H., R. Burgess, T. Mizukami, S. R. Wallis, G. Holland, and C. J. Ballentine (2010), Seawater-derived noble gases and halogens preserved in exhumed mantle wedge peridotite, *Earth Planet. Sci. Lett.*, *294*, 163–172.

Syracuse, E. M., P.E. van Keken, and G. A. Abers (2010), The global range of subduction zone thermal models, *Phys. Earth Planet. Inter.*, *183*, 73–90.

Ueda, H., K. Niida, T. Usuki, K. Hirauchi, M. Meschede, R. Miura, Y. Ogawa, M. Yuasa, I. Sakamoto, T. Chiba, T. Izumino, Y. Kuramoto, T. Azuma, T. Takeshita, T. Imayama, Y. Miyajima, and T. Saito (2011), Seafloor geology of the basement serpentinite body in the Ohmachi Seamount (Izu-Bonin arc) as exhumed parts of a subduction zone within the Philippine Sea. In *Accretionary Prisms and Convergent Margin Tectonicsin the Northwest Pacific Basin* (Y. Ogawa et al. eds.), *Modern Approaches in Solid Earth Sciences*, *8*, 97–128.

Ulmer, P. and V. Trommsdorff (1995), Serpentine stability to mantle depths and subduction-related magmatism, *Science*, *268*, 858–861.

Ulmer, P. and V. Trommsdorff (1999), Phase relations of hydrous mantle subducting to 300 km, In *Mantle Petrology: Field Obervations and High Pressure Experimentation* (Fei Y., C. M. Bertka, and B. O. Mysen, eds.), 259–281.

Wessel, P., and W. H. F. Smith (1998), New, improved version of Generic Mapping

Tools released, *Eos Trans. AGU*, *79*, 579.

Wirth, E. A., and M. D. Long (2012), Multiple layers of seismic anisotropy and a

low-velocity region in the mantle wedge beneath Japan: Evidence from teleseismic

receiver functions, *Geochem. Geophys. Geosyst.*, *13*, Q08005,

doi:10.1029/2012GC004180.

Yoshioka, S., M. Toda, and J. Nakajima (2008), Regionality of deep low-frequency

earthquakes associated with subduction of the Philippine Sea plate along the

Nankai Trough, southwest Japan, *Earth Planet. Sci. Lett.*, *272*, 189–198.

Figure captions

Figure 1. (a) Map view of V_P/V_S at a depth of 30 km [*Matsubara et al.*, 2008; *Matsubara and Obara*, 2011]. Dots show the epicenter at depths of 30–250 km, and brown triangles Quaternary active volcanoes. A blue line represents the profile of the cross section presented in Figure 1b. (b) Vertical cross sections of V_P/V_S (upper panel), V_P (middle panel), and V_S (lower panel) along the profile A–B shown in Figure 1a. The land area is shown by a thick line at the top.

Figure 2. Seismic events (open circles) and stations (reverse triangles) used for this study.

Figure 3. Waveform data and splitting analysis at station N.MYJH. (a) Original waveforms of band-pass filtered two horizontal components. Dashed lines show the time window for particle motion and splitting analysis. (b) Particle motion of two horizontal components. (c) Rotated waveforms of a faster shear wave (upper) and slower one (lower). (d) Contour map of the confidence level. Plus shows the optimum splitting parameters of φ and δt. A contour interval corresponds to the confidence of two times the standard error.

Figure 4. Results of shear wave splitting in this study. (a) Splitting parameters are shown at epicenters (dots). The direction and the length of each bar respectively show the faster shear wave polarization, φ, and the delay time between two split shear waves, δt. A dotted line shows the profile of the cross section portrayed in Figure 4b. (b) Vertical cross section of shear wave splitting results for profile A–B indicated in Figure 4a. Gray and color scales respectively show the V_P/V_S value and the observed delay time. Solid lines and dotted lines respectively denote almost trench-normal polarizations and trench-parallel polarizations. A pink thick line shows the PHS slab surface [*Hirose et al.*, 2008; *Nakajima and Hasegawa*, 2007]. Open squares, open circles, and black triangles respectively denote receivers, events and the volcano front.

Figure 5. Comparison between results of shear wave splitting of which the delay time is less than 0.3 s and the maximum horizontal compressional stress [*Ishise and Oda*, 2009] (black dashed lines). Splitting parameters are shown at the receivers.

Figure 6. Relation between X1–X3 axes and slab geometry.

Figure 7. Pole figure of the observed (dark gray bars) and the theoretical (gray bars)

splitting parameters (only delay time ≥ 0.3 s) at seismic stations N.KORH and N.MYJH. The values of h and L respectively represent the anisotropic layer thickness and the degree of CPO assumed in the calculation. Directions and lengths of bars respectively show faster shear wave polarization φ and the delay time between two split shear waves δt. Concentric circles show the take-off angle of the ray.

Figure 8. Gray zone shows a relation between the anisotropic layer thickness and delay time. Upper and lower limits are based on the strength of anisotropy reported by *Frese et al*. [2003].

Figure 9. Pressure-temperature diagram showing controlling factors of water behavior in the south Kyushu subduction zone. The inferred thermal conditions on the slab surface of the south Kyushu are shown as a green band between the slab surface temperatures of the SW (southwest) Japan and the NE (northeast) Japan [*Peacock and Wang*, 1999] (green lines). Black dotted line represents high V_P/V_S region beneath the south Kyushu area [*Matsubara et al.*, 2008; *Matsubara and Obara*, 2011]. The P-T conditions do not exceed the wet solidus of mantle peridotite [*Green et al.*, 2010]. Trench-normal anisotropy and the development of water-saturated C-type olivine fabric

are inferred in this region. Isopleth of the dihedral angle [*Mibe et al.*, 1999] (gray solid

lines), and the antigorite dehydration reaction boundary [*Ulmer and Trommsdroff*, 1995;

Bromley and Pawley, 2003] (blue lines), and stability of main hydrous minerals in

MORB slab [*Schmit and Poli*, 1998] (red lines) are shown. The antigorite stability and

MORB solidus [*Schmidt and Poli*, 1998] constrain the lower and higher temperature

limits of the south Kyushu subduction geotherm, respectively.

Table captions

Table 1. Elastic constants of olivine [*Abramson et al.*, 1997] used for this study. The

values in parentheses represent the error of the elastic constant.

Table 2. Elastic constants of antigorite [*Bezacier et al.*, 2010] used for this study. The

values in parentheses represent the error of the elastic constant.

Table 3. Correspondence table between the set of the X1, the X2, and the X3 axes and

the set of the a-, the b- and the c-axes of olivine slip systems or antigorite.

Table 1.

Elastic constants (GPa): San Carlos olivine single-crystal, 5.2 GPa, 3.485 g/cm^3					
355.4 (10)	91.3 (24)	89.8 (11)	0.0	0.0	0.0
	228.0 (8)	93.7 (12)	0.0	0.0	0.0
		262.1 (9)	0.0	0.0	0.0
			73.4 (4)	0	0.0
				85.8 (5)	0.0
					89.5 (10)

Table 2.

Elastic constants (GPa) :
Central Cuba antigorite single-crystal, room pressure, 2.62 g/cm^3

208.1 (5.8)	66.4 (1.2)	16.0 (1.8)	0.0	5.5 (0.1)	0.0
	201.6 (4.9)	4.9 (0.5)	0.0	-3.1 (0.1)	0.0
		96.9 (0.9)	0.0	0.0	0.0
			16.9 (0.1)	0	-12.1(0.2)
				18.4 (0.1)	0.0
					65.5 (0.5)

Table 3.

Slip system	X1	X2	X3
A-type	a-axis	c-axis	b-axis
B-type	c-axis	a-axis	b-axis
C-type	c-axis	b-axis	a-axis
E-type	a-axis	b-axis	c-axis
Antigorite	a-axis	b-axis	c-axis

Figure 1. (a) Map view of V_P/V_S at a depth of 30 km [*Matsubara et al.*, 2008; *Matsubara and Obara*, 2011]. Dots show the epicenter at depths of 30–250 km, and brown triangles Quaternary active volcanoes. A blue line represents the profile of the

cross section presented in Figure 1b. (b) Vertical cross sections of V_P/V_S (upper panel), V_P (middle panel), and V_S (lower panel) along the profile A–B shown in Figure 1a. The land area is shown by a thick line at the top.

Figure 2. Seismic events (open circles) and stations (reverse triangles) used for this study.

Figure 3. Waveform data and splitting analysis at station N.MYJH. (a) Original waveforms of band-pass filtered two horizontal components. Dashed lines show the time window for particle motion and splitting analysis. (b) Particle motion of two horizontal components. (c) Rotated waveforms of a faster shear wave (upper) and slower one (lower). (d) Contour map of the confidence level. Plus shows the optimum splitting parameters of φ and δt. A contour interval corresponds to the confidence of two times the standard error.

Figure 4. Results of shear wave splitting in this study. (a) Splitting parameters are shown at epicenters (dots). The direction and the length of each bar respectively show the faster shear wave polarization, φ, and the delay time between two split shear waves,

δt. A dotted line shows the profile of the cross section portrayed in Figure 4b. (b) Vertical cross section of shear wave splitting results for profile A–B indicated in Figure 4a. Gray and color scales respectively show the V_P/V_S value and the observed delay time. Solid lines and dotted lines respectively denote almost trench-normal polarizations and trench-parallel polarizations. A pink thick line shows the PHS slab surface [*Hirose et al.*, 2008; *Nakajima and Hasegawa*, 2007]. Open squares, open circles, and black triangles respectively denote receivers, events and the volcano front.

Figure 5. Comparison between results of shear wave splitting of which the delay time is less than 0.3 s and the maximum horizontal compressional stress [*Ishise and Oda*, 2009] (black dashed lines). Splitting parameters are shown at the receivers.
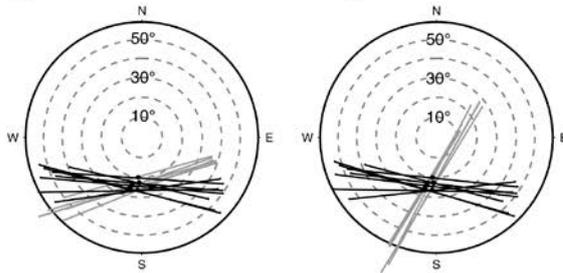
Figure 6. Relation between X1–X3 axes and slab geometry.

N.KORH

A-type olivine h: 30 km L: 60 %   B-type olivine h: 30 km L: 50 %   C-type olivine h: 30 km L: 60 %
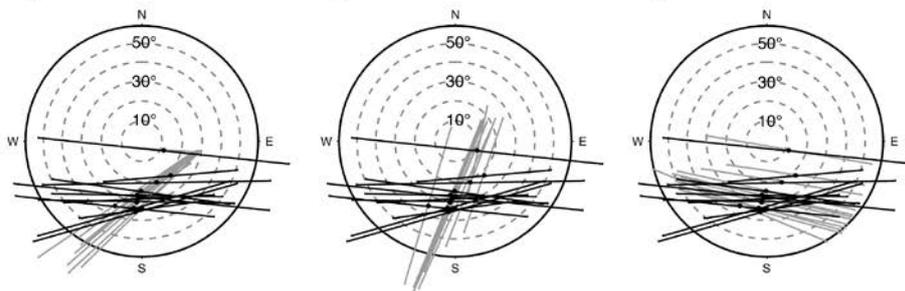
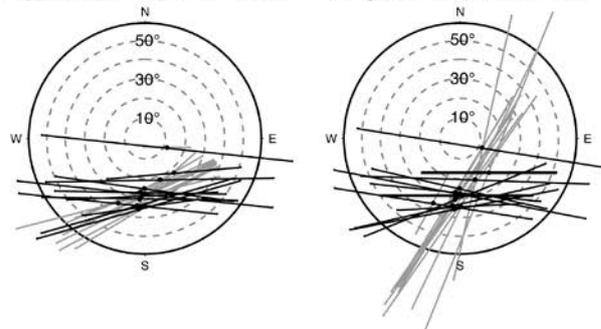E-type olivine h: 35 km L: 60 %   Antigorite h: 15 km L: 40 %

0.2 s

N.MYJH

A-type olivine h: 30 km L: 60 %   B-type olivine h: 30 km L: 50 %   C-type olivine h: 30 km L: 60 %

E-type olivine h: 35 km L: 60 %   Antigorite h: 15 km L: 40 %

0.2 s

Figure 7. Pole figure of the observed (dark gray bars) and the theoretical (gray bars) splitting parameters (only delay time ≥ 0.3 s) at seismic stations N.KORH and N.MYJH.

The values of h and L respectively represent the anisotropic layer thickness and the degree of CPO assumed in the calculation. Directions and lengths of bars respectively show faster shear wave polarization φ and the delay time between two split shear waves δt. Concentric circles show the take-off angle of the ray.
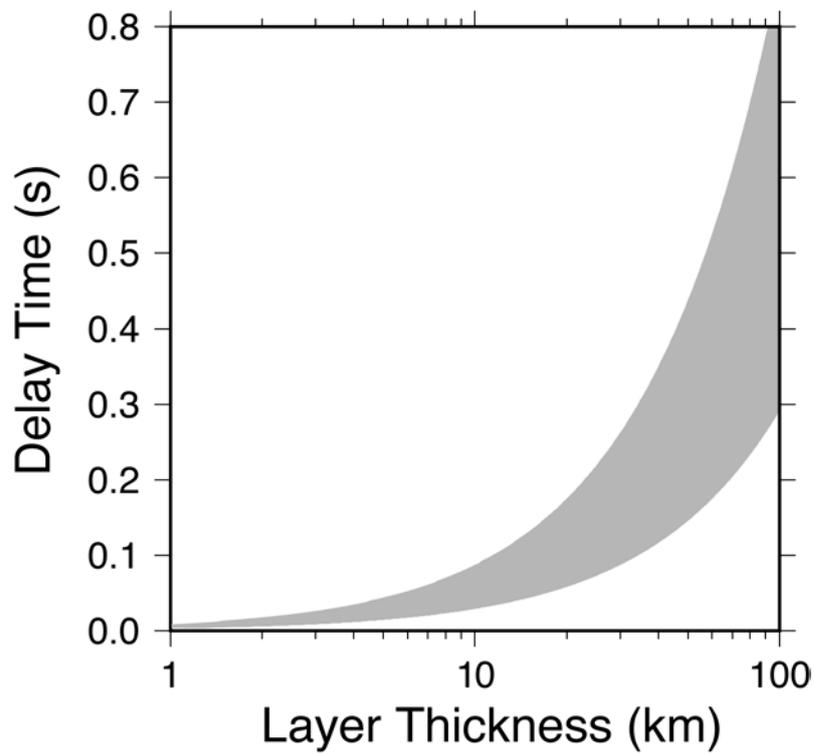
Figure 8. Gray zone shows a relation between the anisotropic layer thickness and delay time. Upper and lower limits are based on the strength of anisotropy reported by *Frese et al.* [2003].
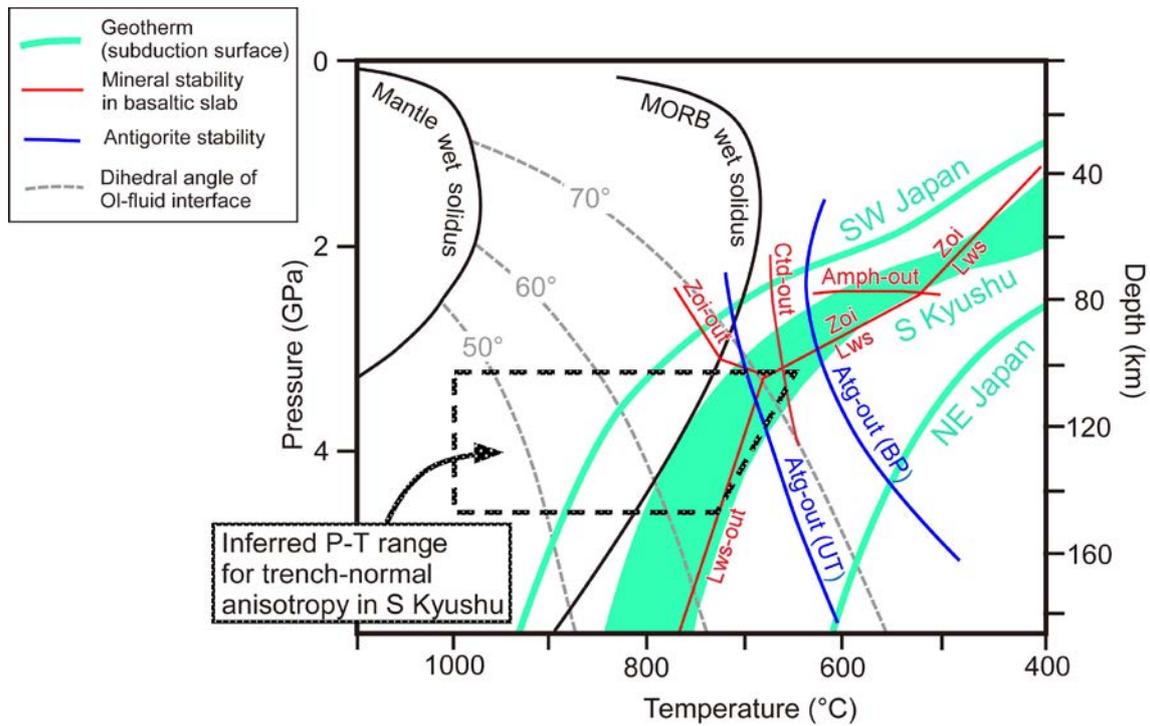
Figure 9. Pressure-temperature diagram showing controlling factors of water behavior in the south Kyushu subduction zone. The inferred thermal conditions on the slab surface of the south Kyushu are shown as a green band between the slab surface temperatures of the SW (southwest) Japan and the NE (northeast) Japan [*Peacock and Wang*, 1999] (green lines). Black dotted line represents high V_P/V_S region beneath the south Kyushu area [*Matsubara et al.*, 2008; *Matsubara and Obara*, 2011]. The P-T conditions do not exceed the wet solidus of mantle peridotite [*Green et al.*, 2010]. Trench-normal anisotropy and the development of water-saturated C-type olivine fabric are inferred in this region. Isopleth of the dihedral angle [*Mibe et al.*, 1999] (gray solid lines), and the antigorite dehydration reaction boundary [*Ulmer and Trommsdroff*, 1995; *Bromley and Pawley*, 2003] (blue lines), and stability of main hydrous minerals in

MORB slab [*Schmit and Poli*, 1998] (red lines) are shown. The antigorite stability and

MORB solidus [*Schmidt and Poli*, 1998] constrain the lower and higher temperature

limits of the south Kyushu subduction geotherm, respectively.